International Journal of Mass Spectrometry 299 (2011) 71–77

Contents lists available at ScienceDirect

International Journal of Mass Spectrometry

journal homepage: www.elsevier.com/locate/ijms

RF ion carpets: The electric field, the effective potential, operational parameters and an analysis of stability

S. Schwarz

National Superconducting Cyclotron Laboratory, Michigan State University, 1 Cyclotron, East Lansing, MI 48824-1321, United States

ARTICLE INFO

Article history:
Received 13 July 2010
Received in revised form
20 September 2010
Accepted 21 September 2010
Available online 29 September 2010

PACS:
29.27.Eg
41.20.Cv
41.85.Ja

Keywords:
Ion transport
Ion carpet
Radiofrequency

ABSTRACT

Analytical solutions for the electric field of radiofrequency (RF) carpets are presented. The formulas have been applied to calculate the effective repulsive potential with the Dehmelt model. The resulting formulas have been used to investigate operational conditions such as the average distance of ions from the carpet in the presence of an attractive static electric field.

The equations of motion of ions in the electric fields have been integrated using the developed formulas to determine the parameter space for carpet operation. The operational parameters have been reduced to three dimensionless parameters and a stability analysis is carried out in these terms.

1. Introduction

Inhomogeneous RF fields are widely used to transport and manipulate ion beams. The most common structures to confine ions in two or three dimensions, e.g., mass filters, ion guides and Paul traps [1], employ quadrupole or higher-multipole RF fields. These electrode structures are commonly used to confine ions either in high vacuum or in the presence of a dilute light buffer gas such as Helium, which dampens the ions' motion [2–4]. The motion of ions in these devices has been studied in great detail and the limiting factors in their operation are well understood, largely owing to their distinct geometry and their usually low and well defined multipolarity.

The effective force confining ions in these structures can be derived from a so-called pseudo or effective potential developed by Dehmelt [5]. It is well known (see Section 3) that the presence of substantial damping can quickly reduce the effective force to an impractical level, where it cannot be recovered by increasing the RF field strength for practical reasons (e.g., discharges). One way to make up for this reduction is to scale down the size of the RF structures. As an example, for a quadrupole rod structure the effective potential scales with the inverse of the inner radius squared.

In order to guide ions in a high-pressure gas environment RF funnels and RF carpets have been developed. The term 'ion funnel' is usually reserved for cone-shaped ion guides made from ring-shaped discrete electrodes [6,7], while RF carpets typically employ stripe electrodes laid out on a printed circuit board [8]. In both devices the electrodes are closely spaced (typical dimensions: sub-mm) to produce locally a sufficiently strong RF electric field that keeps ions away from the material. The electrodes are often biased to generate a DC field that drives the ions in the desired direction towards (in the following called 'push field') and along the RF structure.

Ion funnels have been applied in particular for analytical chemistry. Their use and the use of RF carpets is growing in importance for collection of energetic ions [9–11]. A number of research facilities have implemented so-called gas-stoppers to convert rare isotope beams produced by fast-beam fragmentation or other methods into low-energy beams [9,12–14]. At the National Superconducting Cyclotron Laboratory (NSCL) a linear gas stopper with static extraction fields has been used successfully since 2005 to provide low-energy beams for the LEBIT high-precision mass spectrometer [15]. A new system is being developed to improve ion throughput, efficiency and cleanliness of these devices as more experiments will depend on their performance and reliability. The NSCL will deploy both improved linear gas stoppers and a novel device, called 'cyclotron gas stopper' [16]. The extraction of thermal ions from these devices will

E-mail address: schwarz@nscl.msu.edu.

1387-3806/$ – see front matter © 2010 Elsevier B.V. All rights reserved.
doi:10.1016/j.ijms.2010.09.021

be aided by RF funnels, large-scale RF carpets or combinations of both.

The electric field at the surface of RF funnels and carpets is not dominated by a single multipole and there is no well-developed theory for determining when ion motion is stable. In order to understand ion motion and consequently the operating range of RF carpets, a number of simulations have been reported and also performed at the NSCL. The electric field is usually obtained from field solvers such as Simion [17] and then used for the numerical integration of the equation of motion. This procedure is generally time-consuming, because of the large number of electrodes and the high RF frequency involved, in particular when the damping is not implemented by the usual Stokes-law but the more realistic Monte-Carlo type collisions of ions with gas molecules. In order to survey more quickly the operating range (i.e., ion mass and charge, pressure, RF frequency, RF amplitude, dependence on electrode geometry etc.), an analytical expression for the electric field of an RF carpet was sought. The solution is laid out in Section 2 and in Appendix A and then applied in Section 3 to calculate the effective potential. Fast ion trajectory calculations, based on the derived formulas have been used to predict the operating range in terms of suitable dimensionless parameters. The results are reported in Section 4.

2. Potential and field equations

RF carpets use a cylindrical pattern of concentric stripe electrodes to guide ions towards a center hole for extraction into high vacuum. As can be seen later, the motion of ions across the RF carpet takes place at a small distance from the carpet, comparable to the stripe width. For this reason the near-carpet electric field calculated for a parallel-stripe arrangement will be very similar to the field for cylindrical stripes. To facilitate an analytical calculation, the formulas described below have been derived for parallel stripes.

The top portion of Fig. 1 illustrates the geometry of carpet electrodes in a top view. Conducting stripes with pitch a and separation g are laid out in the x–z-plane. The stripes are assumed to be infinitely long in z-direction and infinitely thin in y-direction. A solution of the Laplace equation for $y > 0$ with the electric field vanishing for $y \to \infty$ is required to describe the ion motion.

In the simplest and most common carpet operation, RF voltages are applied such that two neighboring stripes are out of phase by 180°. The field distribution for one of the two phases can be found by solving the Laplace equation for the boundary conditions shown in the bottom portion of Fig. 1: Some voltage V is applied to every second stripe interleaved with the other stripes carrying no voltage. The voltage between any two stripes is assumed to change linearly. The solution for the other phase is then obtained by offsetting the solution by one pitch a in x-direction and negating the applied voltage. By adding the results for the opposite phases one obtains the full solution for this standard case of operation.

The problem can be generalized by allowing the same voltage V to be applied to every mth electrode with $m-1$ grounded electrodes in between. The standard case discussed before is then simply obtained for $m = 2$. The solution for the electric field produced by this generalized boundary problem is developed in Appendix A.2 leading to the two field components E_x,E_y in Eqs. (A10) and (A15).

While these two somewhat lengthy equations cover the case of $m = 2$, the solutions for this most common case of carpet design can be simplified considerably due to its special symmetry. The formalism for this case is laid out in Appendix A.3 and results in the two field components:

$$E_x = \frac{V}{\gamma a \pi}\left[\arctan\left(\frac{\mathrm{Cx}_-(x_r)}{\mathrm{Shy}(y_r)}\right) - \arctan\left(\frac{\mathrm{Cx}_+(x_r)}{\mathrm{Shy}(y_r)}\right)\right] \tag{1}$$

and

$$E_y = \frac{V}{2\gamma a \pi}\ln\left[\frac{\mathrm{Chy}(y_r)+\mathrm{Sx}_+(x_r)}{\mathrm{Chy}(y_r)-\mathrm{Sx}_+(x_r)}\cdot\frac{\mathrm{Chy}(y_r)-\mathrm{Sx}_-(x_r)}{\mathrm{Chy}(y_r)+\mathrm{Sx}_-(x_r)}\right]. \tag{2}$$

The positions x, y and the gap g have been divided by the pitch a to obtain the dimensionless quantities x_r, y_r and γ, respectively. In addition, three shortcuts have been used for the arguments of the arctan and ln function:

$$\begin{aligned} y_r &:= y/a, \quad x_r := x/a, \quad \gamma := g/a \\ \mathrm{Shy}(y_r) &:= \sinh(\pi y_r) \\ \mathrm{Chy}(y_r) &:= \cosh(\pi y_r) \\ \mathrm{Sx}_\pm(x_r) &:= \sin(\pi[x_r \pm \frac{\gamma}{2}]) \\ \mathrm{Cx}_\pm(x_r) &:= \cos(\pi[x_r \pm \frac{\gamma}{2}]). \end{aligned} \tag{3}$$

The formulas developed so far describe fields that are m-periodic in x-direction. In addition, the solution for a single stripe (with all other stripes grounded) has also been developed. This solution may be used in cases where there is no periodicity and to construct arbitrary solutions including the periodic ones above. The electric field can be obtained from the general m-periodic case for $m \to \infty$. The solution for this case is given in Appendix A.4 with the two field components of Eqs. (A21) and (A23).

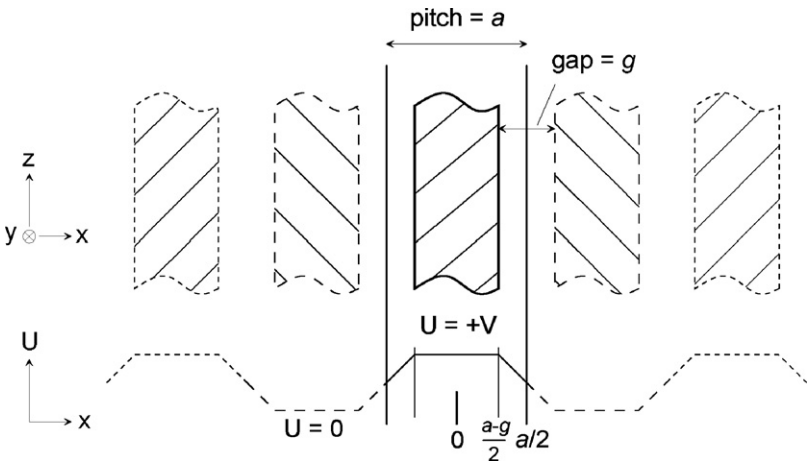

Fig. 1. Boundary conditions for carpet problem (see text).

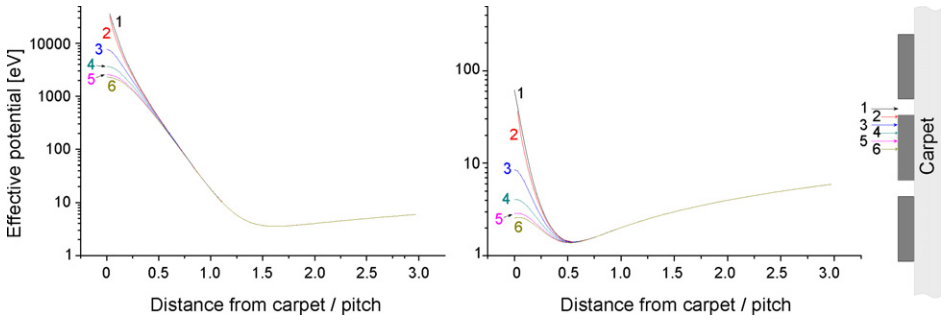

Fig. 2. Effective potential as a function of distance from the carpet surface for six positions between two RF electrodes as indicated on the sketch on the far right. The two panels are for different values of gas pressure above the carpet. Left: 2 mbar, Right: 200 mbar.

3. Effective potential

In this section the effective potential for the standard case of carpet operation ($m = 2$) is evaluated. In this case, the carpet is driven such that amplitudes $+V$ and $-V$ alternate from one stripe to the next, generating twice the field strength calculated from Eqs (1) and (2). The time-averaged effective potential according to Dehmelt is calculated as [5]:

$$V_{\text{eff}} = \frac{q}{4m_i\Omega^2}\vec{E}_0^2 = \frac{q}{4m_i\Omega^2}(E_x^2 + E_y^2), \tag{4}$$

for an ion with mass m_i, driven by a harmonic electric voltage with field amplitude $\vec{E}_0$ and angular frequency Ω. The charge q of the ion equals $Z{\cdot}e$, Z being the number of elementary electronic charges e. Since RF carpets usually operate in a gaseous environment with substantial damping, Eq. (4) needs to be modified to

$$V_{\text{eff, damp}} = \frac{\Omega^2}{\Omega^2 + D^2} V_{\text{eff}}, \tag{5}$$

where D is the damping constant according to $\vec{F}_{\text{damp}} = -m_i D \cdot \vec{v}$, $\vec{v}$ being the velocity vector of the ion. The damping force constant D (unit: 1/s) contains the reduced mobility K_0, temperature T and pressure p as $D = q/m_i{\cdot}1/K_0{\cdot}p/p_0{\cdot}T_0/T$, T_0 and p_0 being standard temperature and pressure. Fig. 2 illustrates the resulting effective potential for six positions between two RF electrodes for a pressure of 2 mbar (left) and 200 mbar (right). An additional constant electric field of 2 V/mm, the push field E_p, is applied in the y-direction that gives rise to the potential wells shown. The minimum effective potential is reduced by about two orders of magnitude in the high pressure case and the minimum moves closer to the carpet surface.

3.1. The location of the minimum in the effective potential

As was shown in Fig. 2, the net effective potential near the carpet's surface exhibits a minimum when an electric field E_p is present that pushes the ion towards the carpet. If the motion of the ion is stable the ion can hover above the carpet's surface near the location of this minimum without striking the carpet surface. While the pseudo-potential cannot tell if an ion motion will be stable, the location of the minimum can give some guidance: an operating point with a calculated minimum in the effective potential close to the carpet will be unlikely to yield stable conditions.

Fig. 2 also shows that the effective potential is almost independent of x, provided the distance y from the surface is large enough. For $y \gg a$ a suitable approximation can be found from the Dehmelt potential at $x_r = 0$, over the center of an electrode, where only E_y (Eq. (2)) contributes. For $x = 0$ and $y_r \gg 0$, the doubled field component E_y from Eq. (2) simplifies to

$$E_y(x_r = 0,\ y_r \gg 0) = \frac{8V}{\gamma a \pi} \sin(\pi\gamma/2)\exp(-\pi y_r). \tag{6}$$

After inserting the required factors the Dehmelt potential is calculated as

$$D(y) = E_p y + \frac{1}{\Omega^2 + D^2}\frac{q}{4m_i}\left(\frac{8V}{\gamma a\pi}\right)^2 \sin^2(\pi\gamma/2)\exp(-2\pi y/a). \tag{7}$$

From the condition that the derivative $\mathrm{d}D/\mathrm{d}y$ vanishes one can easily find the location of the minimum in the effective potential:

$$y_{\min} = -\frac{a}{2\pi}\ln\left(E_p a(\Omega^2 + D^2)\frac{\pi}{8\sin^2(\pi\gamma/2)}\frac{m_i}{q}\left(\frac{\gamma a}{2V}\right)^2\right). \tag{8}$$

A comparison of the correct derivative with this approximation indicates that the approximation is good for approximately $y/a \geq 0.5$, for almost any value of $0 < \gamma < 1$.

3.2. The optimum gap-to-pitch ratio γ

From the location of the minimum in the effective potential, Eq. (8), one can calculate the gap-to-pitch ratio γ that is most effective in countering the pushing field E_p, i.e., that will keep the ions the farthest away from the carpet for a given set of operation conditions. Requiring the derivative of Eq. (8) with respect to γ to vanish leads to the simple condition $\pi\gamma/2 = \tan(\pi\gamma/2)$. This condition is trivially met at $\gamma = 0$, i.e., for vanishing gap size. The minimum in the effective potential only slowly varies with γ. As an example, if the operating parameters are chosen such that the minimum in the effective potential is $y_{\min} = 2a$ for $\gamma = 0$, then even changing γ to 1 will only lower $y_{\min}$ by about 7.2%. For this reason the requirement for (the unrealistic situation of) $\gamma = 0$ is not a stringent one and practical concerns should rather determine γ.

4. Stability—Maximum pushing field

An important factor in the operation of RF carpets is the applied electric field E_p that pushes the ions towards the carpet's surface. This electric field may be deliberately applied to move the ions towards the carpet for transport along the surface or it may be a consequence of space charge built up by a large number of ions in a device with a carpet lining [18,19] (or both). As can be seen from Eqs. (1) to (2), the electric field near the carpet surface is a rather non-linear function that does not allow one to easily infer the repelling power of the carpet from the ion's equation of motion.

The typical carpet operating pressure often exceeds a few tens of mbars. With this substantial damping the ion trajectories typically look like the one shown in Fig. 3, when E_p is large enough to drive the ion onto the carpet and the ion will hit the surface in the middle of one of the stripes. Thus the electric field component E_y at $x = 0$ from Eq. (2) will determine if an ion hits the surface or not. The simplified version of Eqs. (2) and (6), can be used to get an approximate description of the repelling force of the carpet. While this equation was derived for large y_r, it is in fact a very good approximation even for small values of y_r, if the gap-to-pitch parameter is

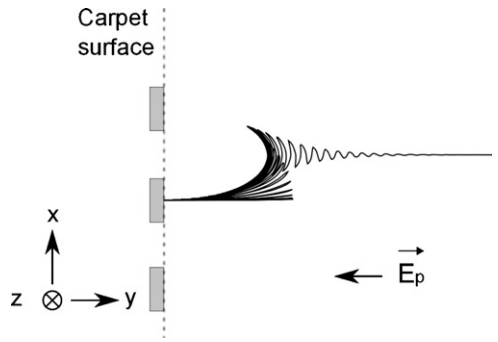

Fig. 3. Typical ion trajectory in the presence of strong damping and if the 'pushing field' E_p is large enough to move the ion close to the carpet. In this case the ion is likely to hit the carpet in the center of one of the electrodes.

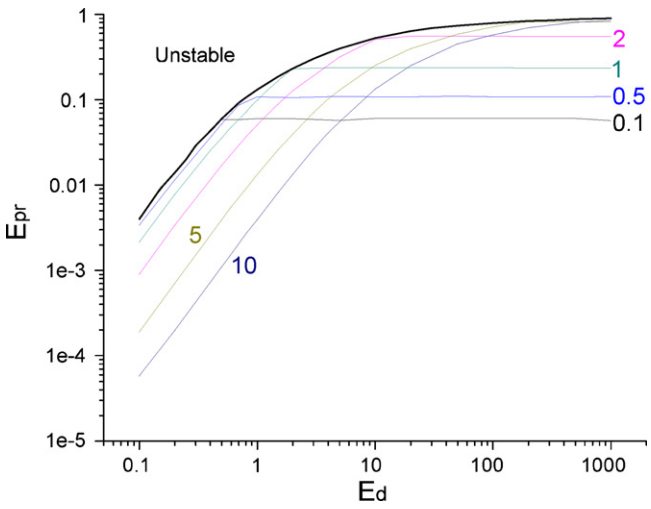

Fig. 4. RF carpet stability diagram for the dimensionless RF field component E_d and push field E_{pr} with the reduced damping parameter κ.

near 3/4. With this approximation for E_y, the equation of motion in terms of time, t, can be written:

$$m_i \frac{d^2y}{dt^2} = q \cdot \frac{8V}{\gamma a \pi} \sin(\pi\gamma/2) \exp(-\pi y/a) \cdot \cos(\Omega t) - qE_p - m_i D \frac{dy}{dt}. \quad (9)$$

In order to understand the motion described by this differential equation, it is advantageous to turn it into an equivalent dimensionless equation with minimum number of parameters. By defining $y_\pi = y\pi/a$ and $\xi = \Omega t$ Eq. (9) is easily transformed into:

$$\frac{d^2y_\pi}{d\xi^2} = E_d \exp(-y_\pi) \cos(\xi) - E_{pr} - \kappa \frac{dy_\pi}{d\xi}, \quad (10)$$

with three remaining parameters

$$E_d = \frac{q}{m_i} \frac{1}{\Omega^2} \frac{8V}{\gamma a^2} \sin(\pi \frac{\gamma}{2}), \quad E_{pr} = \frac{q}{m_i} \frac{1}{\Omega^2} \frac{\pi}{a} E_p, \quad \text{and} \quad \kappa = D/\Omega \quad (11)$$

Eq. (10) has been numerically integrated for a number of values E_d and κ and in each integration the parameter E_{pr} was adjusted so that the minimum value of y_π was zero – this corresponds to the situation that an ion would just touch the carpet – or the minimum that would not let the ion motion become unstable. The results of these calculations are shown in Fig. 4.

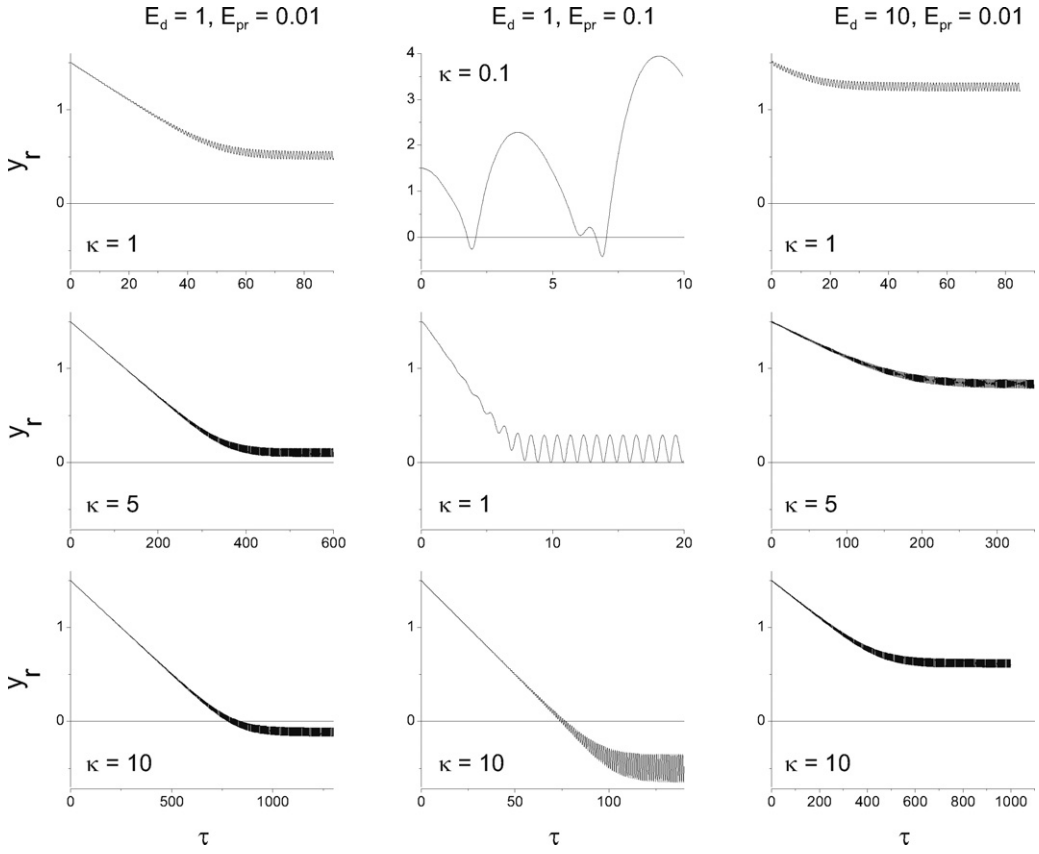

Fig. 5. Sample trajectories. The panels show the reduced coordinate y_r as a function of time, measured in multiples of the RF period τ. Columns have the same field strengths E_d and E_{pr}, whereas the top two rows differ in the damping term κ.

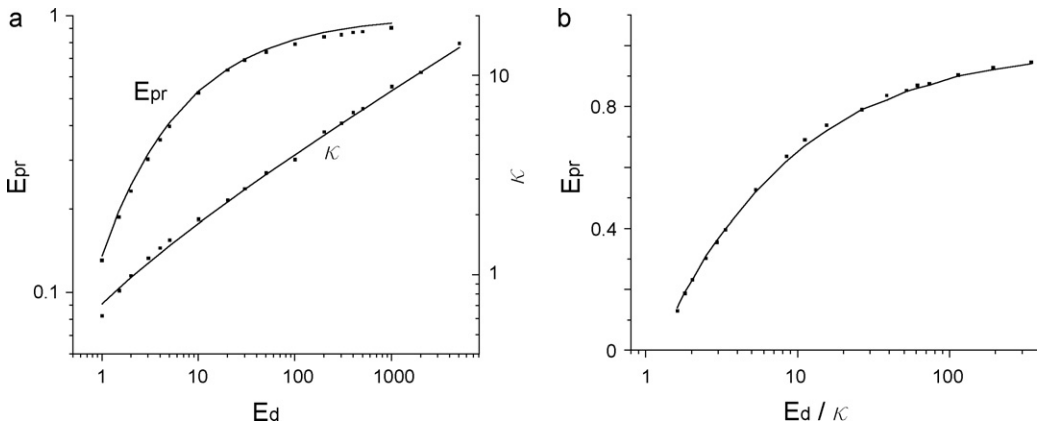

Fig. 6. Stability limits. Panel (a) shows both the limiting line for the reduced push field E_{pr} as a function of E_d (same as the thick line in Fig. 4) and the variation of κ along that line. Panel (b) shows E_{pr} as a function of the ratio of E_d to κ. (See text).

Points with equal values of κ are joined by lines. For certain combinations of E_d and κ no stable solution with the required boundary condition was found. Instability was observed, if E_d was larger than the values connected by the thick line, regardless of the damping term κ. Curves with equal κ increase sharply with E_d up to a maximum E_{pr} and become independent of E_d. On the rising branch of these curves, the trajectories touch $y = 0$, whereas on the horizontal branch the minimum y increases with E_d. The line separating stable from unstable motion is given by the condition that the ion motion just touches the carpet ($y = 0$) and that κ is small enough that the motion becomes unstable at this point.

Fig. 5 illustrates some of the trajectories that contribute to the 'stability'-diagram (Fig. 4). The figure shows the reduced coordinate y_r as a function of time, given in multiples of the RF-period for nine combinations of E_d and E_{pr} and κ. All of the trajectories start out with the same initial condition $y_r = 1.5$ and zero velocity. The first column ($E_d = 1$, $E_{pr} = 0.01$) shows situations where the motion relaxes to a stable solution, but the increase in the damping term κ causes the minimum to drop below the carpet surface ($y_r = 0$). The second column ($E_d = 1$, $E_{pr} = 0.1$) illustrates a set of pathological parameters, where increasing the damping term κ causes the motion to go from unstable ($\kappa = 0.1$) to a motion inside the carpet. The last column ($E_d = 10$, $E_{pr} = 0.1$) illustrates a set of useful parameters, where the three damping terms κ cause stable motion with different distances from the carpet surface. As an example, the $E_d = 10$, $E_{pr} = 0.01$, $\kappa = 1$ case reflects the situation for an $m = 70\,\mu$ ion on a carpet with U = 100 V, $a = 0.2$ mm, $\gamma = 0.5$, $\Omega/2\pi = 10$ MHz, $p_{He} = 100$ mbar and a pushing field of 10 V/cm at room temperature.

The calculated points defining the boundary of stability (or usefulness) from Fig. 4 are shown again in Fig. 6(a) together with a line to guide the eye.

In the range shown here, the points roughly follow the expression $E_{pr} = \exp(-2/\sqrt{E_d})$. Fig. 6(a) also shows the calculated κ values that were necessary to arrive at the stability line as explained above with a trend line to guide the eye. In order to consolidate the conditions for the three parameters E_{pr}, E_d and κ the relation of E_{pr} with E_d/κ has been calculated and is shown in Fig. 6(b). These points follow the empirical relation

$$E_{pr} = 1 - 1.09/\sqrt{E_d/\kappa}, \tag{12}$$

which is shown by the solid line. From the definition of D and the reduced parameters (see Eq. (11)) it can be seen that E_d/κ does not depend on the mass-over-charge ratio m_i/q while E_{pr} does. Thus, is easy to turn Eq. (12) into a condition for a mass-cutoff or to calculate the maximum pushing field E_p as a function of the operating parameters.

5. Summary and outlook

Analytical solutions for the electric field of RF carpets have been developed. The resulting formulas have been used to calculate the effective potential near the carpet surface and to explore the useful parameter space for carpet operation. The operation parameters have been consolidated into three parameters related to the RF-field, the push-field and damping, which determine the stability of ion motion near the carpet surface.

Ion trajectory simulations are currently underway using the developed field formula, but with the Stokes-law damping replaced by realistic Monte-carlo type collisions of ions with gas molecules. A lowering of the applicable push field compared to relation (12) can be expected, if the ion moves very close to the carpet surface. In such cases, a sudden change of the ion's velocity vector due to a collision with a buffer gas molecule may not be 'averaged out' fast enough in subsequent collisions with gas molecules to prevent the ion from hitting the carpet. These effects will be studied and calculated transport efficiencies will be compared to experimental results from the NSCL RF carpet test stand [20].

Acknowledgments

The author wishes to thank G. Bollen and D. J. Morrissey for valuable discussions and for the proofreading of the manuscript; the author acknowledges the support by the US Department of Energy Contract DE-FG02-06ER41413.

Appendix A. The electric field produced by the carpet

A.1. The potential

Because of the periodic nature of the problem and with the z-axis placed in the middle of one voltage-carrying electrode the potential can be expanded as a cosine series

$$\phi(x, y) = \sum_{n=0}^{\infty} A_n \exp\left(-\frac{2n\pi}{m} y_r\right) \cdot \cos\left(\frac{2n\pi}{m} x_r\right). \tag{A1}$$

To shorten notation and simplify calculations the dimensionless coordinates $x_r = x/a$ and $y_r = x/a$ have been introduced. For the same reason the gap size g will be expressed as the gap-to-pitch ratio

$\gamma = g/a$. Making use of the symmetry of the problem, the Fourier coefficients A_n, $n \geq 1$ are calculated as

$$A_n = \frac{2}{m} \cdot 2 \cdot V \int_0^{m/2} \phi(x,0) \cos\left(\frac{2n\pi}{m} x_r\right) dx_r. \tag{A2}$$

Inserting the boundary conditions as discussed above, this equation becomes

$$A_n = \frac{4V}{m} \left[\int_0^{(1-\gamma)/2} \cos\left(\frac{2n\pi x_r}{m}\right) dx_r + \int_{(1-\gamma)/2}^{(1+\gamma)/2} \cos\left(\frac{2n\pi x_r}{m}\right) \times \left(\frac{1}{2} - \frac{x_r - 1/2}{\gamma}\right) dx_r \right]. \tag{A3}$$

The two arguments can easily be integrated and the Fourier components simplify to

$$A_n = \frac{2Vm}{\pi^2 n^2 \gamma} \sin\left(\frac{n\pi}{m}\right) \sin\left(\frac{n\pi}{m}\gamma\right). \tag{A4}$$

Inserting this result back in Eq. (A1) gives the expansion for the voltage without the constant term from $n = 0$:

$$\phi_{n>0} = \frac{2Vm}{\pi^2 \gamma} \sum_{n=1}^{\infty} \frac{1}{n^2} \exp\left(-\frac{2n\pi}{m} y_r\right) \sin\left(\frac{n\pi}{m}\right) \sin\left(\frac{n\pi\gamma}{m}\right) \times \cos\left(\frac{2n\pi x_r}{m}\right). \tag{A5}$$

The term from $n = 0$, i.e., the average potential far above the carpet's surface ($y \to \infty$), is readily calculated as

$$\phi_{n=0} = \int_0^{m/2} \phi(x_r, 0) dx_r = \frac{V}{m}. \tag{A6}$$

For quick evaluation it would be nice to have the potential (i.e., the sum of (A5) and (A6)) in closed form. A somewhat similar problem is treated in Jackson's textbook on electrodynamics [21], where he uses a relation between the arctan-function and a series expansion $\sum_{n=\text{odd}} Z^n/n$ of a complex function Z to convert his expanded formula into a closed solution. The main difference from our problem to Jackson's is the $1/n^2$ in the sum of Eq. (A5), which does not allow a direct application of Jackson's technique.

A.2. General periodic solution

The required information for both the ions' motion and the effective potential is the electric field, so it is more promising to find a closed solution for $-((\partial\phi(x,y)/\partial x), (\partial\phi(x,y)/\partial y))$ rather than the potential distribution ϕ. Differentiation of Eq. (A5) for the variable x yields:

$$E_x(x_r, y_r) = \frac{4V}{\gamma a \pi} \sum_{n>0} \frac{1}{n} \exp\left(-\frac{2n\pi}{m} y_r\right) \sin\left(\frac{n\pi}{m}\right) \sin\left(\frac{n\pi\gamma}{m}\right) \times \sin\left(\frac{2n\pi x_r}{m}\right). \tag{A7}$$

With the identity

$$\sin(b)\sin(c)\sin(d) = -1/4\, \Im(e^{i(b+c+d)} - e^{i(b+c-d)} - e^{i(b-c+d)} + e^{i(b-c-d)}) \tag{A8}$$

for some arbitrary arguments b,c,d one obtains

$$E_x(x_r, y_r) = -\frac{V}{\gamma a \pi} \Im\left(\sum_{n>0} \frac{1}{n} e^{i\frac{n\pi}{m}(1+\gamma+2x_r+2iy_r)} - \ldots - \ldots + \ldots\right), \tag{A9}$$

where the ellipses denote the remaining terms according to Eq. (A8). Now one can use the series expansion $-\ln(1-Z) = \sum_{n>0} Z^n/n$ for some complex quantity Z together with the identity $\Im\ln(Z) = \arg(Z)$ to arrive at the closed solution

$$E_x(x_r, y_r, m) = \frac{V}{\gamma a \pi} \arctan\left(\frac{4\mathrm{SP}(x_r, y_r, m)}{\mathrm{CS}(x_r, y_r, m) - 4\mathrm{CP}(x_r, y_r, m)}\right). \tag{A10}$$

To shorten notation three definitions have been used:

$$\begin{aligned}
\mathrm{SP}(x_r, y_r, m) &:= \sin\left(\frac{\pi}{m}\right) \sin\left(\frac{\pi\gamma}{m}\right) \sin\left(\frac{2\pi x_r}{m}\right) \sinh\left(\frac{2\pi y_r}{m}\right) \\
\mathrm{CS}(x_r, y_r, m) &:= \cos\left(\frac{2\pi}{m}\right) + \cos\left(\frac{2\pi\gamma}{m}\right) + \cos\left(\frac{4\pi x_r}{m}\right) + \cosh\left(\frac{4\pi y_r}{m}\right) \\
\mathrm{CP}(x_r, y_r, m) &:= \cos\left(\frac{\pi}{m}\right) \cos\left(\frac{\pi\gamma}{m}\right) \cos\left(\frac{2\pi x_r}{m}\right) \cosh\left(\frac{2\pi y_r}{m}\right)
\end{aligned} \tag{A11}$$

In order to obtain the electric field perpendicular to the surface of the carpet, Eq. (A5) is differentiated for the variable y:

$$E_y(x_r, y_r) = \frac{4V}{\gamma a \pi} \sum_{n>0} \frac{1}{n} \exp\left(-\frac{2n\pi}{m} y_r\right) \sin\left(\frac{n\pi}{m}\right) \sin\left(\frac{n\pi\gamma}{m}\right) \times cos\left(\frac{2n\pi x_r}{m}\right). \tag{A12}$$

In this case one can use the identity

$$\cos(b)\sin(c)\sin(d) = \frac{-1}{4} \Re(e^{i(b+c+d)} - e^{i(b+c-d)} - e^{i(b-c+d)} + e^{i(b-c-d)}) \tag{A13}$$

to arrive at

$$E_y(x_r, y_r) = -\frac{V}{\gamma a \pi} \Re\left(\sum_{n>0} \frac{1}{n} e^{i\frac{n\pi}{m}(2x_r+1+\gamma+2iy_r)} - \ldots - \ldots + \ldots\right), \tag{A14}$$

where the ellipses denote the remaining terms according to Eq. (A13). Now one can use again the series expansion $-\ln(1-Z) = \sum_{n>0} Z^n/n$ as before, but with the identity $\Re\ln(Z) = 1/2 \ln\left(|Z|^2\right)$ to obtain the closed solution

$$E_y(x_r, y_r, m) = \frac{V}{2\gamma a \pi} \ln\left(\frac{(\mathrm{CS}_2 - 4\mathrm{CP})^2 + 16\mathrm{SP}_2^2}{4\mathrm{CA}_-^2 \cdot \mathrm{CA}_+^2}\right). \tag{A15}$$

Again a few functions of x_r, y_r and m have been introduced to simplify notation:

$$\begin{aligned}
\mathrm{CS}_2(x_r, y_r, m) &:= \cos\left(\frac{4\pi x_r}{m}\right) + \cos\left(\frac{2\pi}{m}\right) + \cos\left(\frac{2\pi\gamma}{m}\right) + \cosh\left(\frac{4\pi y_r}{m}\right) \\
\mathrm{SP}_2(x_r, y_r, m) &:= \sin\left(\frac{2\pi x_r}{m}\right) \sin\left(\frac{\pi}{m}\right) \sin\left(\frac{\pi\gamma}{m}\right) \sinh\left(\frac{2\pi y_r}{m}\right) \\
\mathrm{CA}_\pm(x_r, y_r, m) &:= \cos\left(\frac{\pi}{m}(2x_r \pm 1 \mp \gamma)\right) - \cosh\left(\frac{2\pi y_r}{m}\right)
\end{aligned} \tag{A16}$$

A.3. Special case for $m = 2$

While Eqs. (A10) and (A15) cover the case of $m = 2$, the solutions for this most common case of carpet operation can be simplified further. Due to the special symmetry only the odd terms in Eqs. (A9) and (A14) contribute in this case. For the field component in

x-direction Eq. (A9) reduces to

$$E_x(x_r, y_r) = -\frac{V}{\gamma a \pi} \Im \left(\sum_{\text{odd}} \frac{1}{n} e^{i\frac{n\pi}{2}(1+\gamma+2x_r+2iy_r)} - \ldots - \ldots + \ldots \right). \tag{A17}$$

This can be brought into closed form with the identity [21]

$$\Im \left(\sum_{n=\text{odd}}^{\infty} \frac{Z^n}{n} \right) = \frac{1}{2} \arctan \left(\frac{2\Im(Z)}{1-|Z|^2} \right) \tag{A18}$$

and the result is the simple expression given in Eq. (1).

For the field component E_y Eq. (A14) reduces to

$$E_y(x_r, y_r) = -\frac{V}{\gamma a \pi} \Re \left(\sum_{\text{odd}} \frac{1}{n} e^{i\frac{n\pi}{2}(1+\gamma+2x_r+2iy_r)} - \ldots - \ldots + \ldots \right). \tag{A19}$$

Here the relation

$$\Re \left(\sum_{n=\text{odd}}^{\infty} \frac{Z^n}{n} \right) = \frac{1}{4} \ln \left(\frac{1+2\Re(Z)+|Z|^2}{1-2\Re(Z)+|Z|^2} \right) \tag{A20}$$

can be used, which is obtained by combining $\Re \ln(Z) = \frac{1}{2} \ln |Z|^2$ and $\sum_{\text{odd}} \frac{Z^n}{n} = \frac{1}{2} \ln \left(\frac{1+Z}{1-Z} \right)$. After consolidating the emerging four logarithms the result for E_y comes out, which is given in Eq. (2).

A.4. The single stripe

To complete the formalism the electric field produced by a single stripe with all other electrodes grounded will be developed. The electric field in this case can be obtained from the general cases discussed above for $m \to \infty$.

To obtain the electric field component in x-direction, one needs to inspect the argument of the arctan-function in Eq. (A10). Because of the product of the three sine and the hyperbolic sine functions involving π/m in the nominator, the denominator has to be expanded up to fourth order in π/m. In the limit of $m \to \infty$ higher orders then cancel out. After consolidating the remaining low-order terms one obtains for the electric field component in x

$$E_x(x_r, y_r) = \frac{V}{\gamma a \pi} \arctan \left(\frac{32\gamma x_r y_r}{\text{DE}_x(x_r, y_r)} \right), \tag{A21}$$

where the denominator in the argument is now simply

$$DE_x(x_r, y_r) = (1-\gamma^2)^2 - 8(x_r^2 - y_r^2)(1+\gamma^2) + 16(x_r^2 + y_r^2)^2. \tag{A22}$$

The electric field component in y-direction is obtained similarly after inspection of the argument of the In-function in Eq. (A15). Here the product of the three sine and the hyperbolic sine functions is squared and so one has to expand both nominator and denominator to eighth order in π/m before higher orders drop out for $m \to \infty$. After accounting for all the lower-order terms the electric field component in y comes out as

$$E_y(x_r, y_r) = \frac{V}{2\gamma a \pi} \ln \left(\frac{AY_+(x_r, y_r)}{AY_-(x_r, y_r)} \right), \tag{A23}$$

where the argument of the In-function has been written in terms of the functions

$$AY_\pm(x_r, y_r) = ((1 \pm \gamma)^2 - 4x_r^2)^2 + 8((1 \pm \gamma)^2 + 4x_r^2)y_r^2 + 16y_r^4. \tag{A24}$$

References

[1] For an overview of ion traps, see e.g., P.K. Ghosh, *Ion traps*, International Series of Monographs in Physics, Oxford University Press (1995).
[2] H.G. Dehmelt, Radiofrequency spectroscopy of stored ions—II: Spectroscopy, Adv. At. Mol. Phys. 5 (1969) 109–154.
[3] G.C. Stafford Jr., P.E. Kelley, J.E.P. Syka, W.E. Reynolds, J.F.J. Todd, Recent improvements in and analytical applications of advanced ion trap technology, Int. J. Mass Spectrom. Ion Processes 60 (1984) 85–98.
[4] M. Lunney, R. Moore, Cooling of mass-separated beams using a radiofrequency quadrupole ion guide, Int. J. Mass Spectrom. 190/191 (1999) 153–160.
[5] H.G. Dehmelt, Radiofrequency spectroscopy of stored ions—I: Storage, Adv. At. Mol. Phys. 3 (1967) 53–72.
[6] S.A. Shaffer, K. Tang, G.A. Anderson, D.C. Prior, H.R. Udseth, R.D. Smith, A novel ion funnel for focusing ions at elevated pressure using electrospray ionization mass spectrometry, Rapid Commun. Mass Spectrom. 11 (1997) 1813–1817.
[7] T. Kim, A.V. Tolmachev, R. Harkewicz, D.C. Prior, G. Anderson, H.R. Udseth, R.D. Smith, T.H. Bailey, S. Rakov, J.H. Futrell, Design and implementation of a new electrodynamic ion funnel, Anal. Chem. 72 (2000) 2247–2255.
[8] M. Wada, Y. Ishida, T. Nakamura, Y. Yamazaki, T. Kambara, H. Ohyama, Y. Kanai, T.M. Kojima, Y. Nakai, N. Ohshima, A. Yoshida, T. Kubo, Y. Matsuo, Y. Fukuyama, K. Okada, T. Sonoda, S. Ohtani, K. Noda, H. Kawakami, I. Katayama, Slow RI-beams from projectile fragment separators, Nucl. Instrum. Methods B204 (2003) 570.
[9] G. Savard, J. Clark, C. Boudreau, F. Buchinger, J. Crawford, H. Geissel, J. Greene, S. Gulick, A. Heinz, J. Lee, A. Levand, M. Maier, G. Münzenberg, C. Scheidenberger, D. Seweryniak, K. Sharma, G. Sprouse, J. Vaz, J. Wang, B. Zabransky, Z. Zhou, Development and operation of gas catchers to thermalize fusion–evaporation and fragmentation products, Nucl. Instrum. Methods B204 (2003) 582–586.
[10] S. Eliseev, M. Block, A. Chaudhuri, Z. Di, D. Habs, F. Herfurth, H.-J. Kluge, J. Neumayr, W. Plaß, C. Rauth, P. Thirolf, G. Vorobjev, Z. Wang, Extraction efficiency and extraction time of the SHIPTRAP gas-filled stopping cell, Nucl. Instrum. Methods B258 (2007) 479–484.
[11] M. Petrick, W. Plaß, K.-H. Behr, A. Brünle, L. Caceres, J. Clark, Z. Di, S. Elisseev, M. Facina, A. Fettouhi, H. Geissel, W. Hüller, M. Huyse, C. Karagiannis, B. Kindler, R. Knöbel, Y. Kudryavtsev, J. Kurcewicz, T. Levant, Y. Litvinov, B. Lommel, M. Maier, D. Morrissey, G. Münzenberg, M. Portillo, G. Savard, C. Scheidenberger, P. Van Duppen, H. Weick, M. Winkler, B. Zabransky, Online test of the FRS ion catcher at GSI, Nucl. Instrum. Methods B266 (2008) 4493–4497.
[12] M. Wada, Deceleration and cooling of radioactive isotope beams – from *GeV to μeV*, Nucl. Instrum. Methods A532 (2004) 40–47.
[13] D.J. Morrissey, Extraction of thermalized projectile fragments from gas, Eur. Phys. J. Special Topics 150 (2007) 365–366.
[14] J. Neumayr, L. Beck, D. Habs, J. Heinz, S. Szerypo, P. Thirolf, V. Varentsov, F. Voit, D. Ackermann, D. Beck, Z. Block, M. Di, S. Eliseev, H. Geissel, F. Herfurth, F. Heßberger, S. Hofmann, H.-J. Kluge, M. Mukherjee, G. Münzenberg, W. Petrick, M. Quint, S. Rahaman, C. Rauth, D. Rodrguez, C. Scheidenberger, G. Sikler, Z. Wang, C. Weber, W. Plaß, M. Breitenfeldt, A. Chaudhuri, G. Marx, L. Schweikhard, A. Dodonov, Y. Novikov, M. Suhonen, The ion-catcher device for SHIPTRAP, Nucl. Instrum. Methods B244 (2006) 489–500.
[15] L. Weissman, D.J. Morrissey, G. Bollen, D. Davies, E. Kwan, P. Lofy, P.A. Schury, S. Schwarz, C. Sumithrarachchi, T. Sun, R. Ringle, Conversion of 92 Mev/u ^{38}Ca/^{37}K projectile fragments into thermalized ion beams, Nucl. Instrum. Methods A540 (2005) 245.
[16] G. Bollen, D.J. Morrissey, S. Schwarz, A study of gas-stopping of intense energetic rare isotope beams, Nucl. Instrum. Methods A550 (2005) 27–38.
[17] D.A. Dahl, SIMION for the personal computer in reflection, Int. J. Mass Spectrom. 200 (2000) 3–25, As of 2010, available from: http://simion.com/.
[18] A. Takamine, M. Wada, Y. Ishida, T. Nakamura, K. Okada, Y. Yamazaki, T. Kambara, Y. Kanai, T. Kojima, Y. Nakai, N. Oshima, A. Yoshida, T. Kubo, S. Ohtani, K. Noda, I. Katayama, P. Hostain, V. Varentsov, H. Wollnik, Space-charge effects in the catcher gas cell of an RF ion guide, Rev. Sci. Instrum. 76 (2005) 103503.
[19] Y. Batygin, G. Bollen, C. Campbell, F. Marti, D. Morrissey, G. Pang, S. Schwarz, Effect of space charge on extraction efficiency of ions in cyclotron gas stopper, in: Proc. Particle Accelerator Conference, 2009, Joint Acc. Conf. Website, tbp 2010.
[20] G.K. Pang, G. Bollen, C.M. Campbell, D.J. Morrissey, S. Schwarz, Nuclear instruments and methods, in preparation.
[21] J.D. Jackson, Classical Electrodynamics, John Wiley and sons, 1975, pp. 71–74.